# Theoretical Study on the Mechanism of the $^1CHF+N_2O$ Reaction

**Jian-jun Liu, Yi-hong Ding, Ji-kang Feng,* and Chia-chung Sun**

*State Key Laboratory of Theoretical and Computational Chemistry, Jilin University, Changchun, Jilin 130023, P. R. China*

*Received: November 12, 2001; In Final Form: January 16, 2002*

The complex singlet potential energy surface of the $CHFN_2O$ system is investigated at the QCISD(T)/6-311G(d,p)//B3LYP/6-31G(d,p) level in order to explore the possible reaction mechanism of $^1CHF$ radical with $N_2O$. Twenty-eight minimum isomers and sixty-four transition states are located. For the most relevant reaction pathways, the high-level QCISD(T)/6-311G(2df,p) single-point calculations are performed at the MP2/6-311G(d,p) geometries to accurately determine the energetics. In various possible initial association ways, the end-N attack leading to $HFCN_2O$ **a**$_1$ is the most feasible pathway with the barrier of 13.5 kcal/mol, whereas for the other attack ways, each involves a higher barrier and thus may not be of significance even at very high temperatures. Starting from $HFCN_2O$ **a**, the most favorable reaction pathway is the almost barrierless dissociation of *trans*-$HFCN_2O$ **a** leading to product **P**$_1$ HFCN+NO via the direct N−N bond cleavage. A comparable pathway is the ring-closure of *cis*-$HFCN_2O$ **a**$_3$ leading to four-membered ring isomer **b** followed by the direct dissociation to **P**$_4$ $N_2$+HFCO. The less and least competitive pathways are the concerted F-shift and N−N bond rupture to **P**$_2$ HCN+FNO as well as the concerted H-shift and N−N bond cleavage to **P**$_3$ FCN+HNO, respectively. However, these primary products **P**$_1$, **P**$_2$, **P**$_3$, and **P**$_4$ cannot further dissociate due to thermodynamical and kinetic factors. By comparison, it is found that the B3LYP-calculated and MP2-calculated results are generally in agreement. In addition, the discrepancies and similarity between the title reaction and analogous $^1CH_2+N_2O$ reaction are discussed. The present paper may assist in future experimental identification of the product distributions for the title reaction and may be helpful for understanding the halogenated carbene chemistry.

## 1. Introduction

The halogenated carbenes are important intermediates in the incineration of fluorine- and chlorine-containing wastes and in the combustion inhibition mechanisms of fluorine-, bromine-, and iodine-containing flame suppressants.[1] A large number of experimental investigations have been carried out on the CHF reactions.[2−9] It is worthwhile to notice that for any combustion systems, $N_2O$ is inevitably produced. Particularly, it is known to be intermediate in the conversion in flames of fuel-N and atmospheric $N_2$ to the harmful pollutant NO.[10] One effective way to minimize the $NO_x$ pollutant is to chemically reduce $N_2O$ in order to prevent its further conversion to NO. Obviously, the key reaction of $^1CHF$ with $N_2O$ plays an important role in reducing $NO_x$ pollutant in the combustion process.

However, to our best knowledge, only one experimental study has been reported on the rate constants of the $^1CHF$ reactions with $N_2O$.[11] The measured rate constant of the $^1CHF+N_2O$ reaction at room temperature was $(2.55 \pm 0.15) \times 10^{-12}$ cm$^3$ molecule$^{-1}$ s$^{-1}$. Clearly, the title reaction is much slower than the analogous $^1CH_2+N_2O$ reaction with the rate constant $k = (6.31 \pm 0.67) \times 10^{-11}$ cm$^3$ molecule$^{-1}$ s$^{-1}$ measured by Koch et al.[12] It indicates that $^1CHF$ reactivity with $N_2O$ decreases because the F atom strongly attracts a lone pair of electrons located at the C atom. Further, the reduction of $^1CHF$ reactivity may lead to the mechanism discrepancy between the $^1CHF$ and $^1CH_2$ reaction with $N_2O$.

Principally, the reactions of $^1CHF$ and $^1CH_2$ with the same species can proceed via different mechanisms. A typical example is $^1CHF+NO$[13−15] and $^1CH_2+NO$,[16−25] (both $^1CH_2+NO$ and $^3CH_2+NO$ are the same doublet potential energy surface) which has been considered as the key processes for modeling nitrogen chemistry in combustion and has been the subject of numerous theoretical and experimental investigations. Particularly, theoretical calculations showed that the product distribution of the $^1CHF+NO$ reaction was in marked difference from that of $^1CH_2+NO$ reaction, although the potential energy surface features of the two reactions are very similar. Then, it is very reasonable for us to suggest that the mechanism of the title $^1CHF+N_2O$ reaction may be different from that of the $^1CH_2+N_2O$ reaction. However, no theoretical studies on the title reaction have been carried out up to now. Whether the two reactions proceed via different mechanisms or not waits to be tested.

Moreover, a detailed study on the potential energy surface (PES) is desirable, at least from a theoretical viewpoint, to explore the product distribution of the title reaction. The present work assists the experimental product observation in the future laboratory studies. In addition, $^1CHF$, as a simplest halogenated carbene, may represent a good model of $N_2O$ reactions with $^1CHCl$, $^1CHBr$, and $^1CHI$.

## 2. Computational Methods

All calculations are carried out using the Gaussian 98 program.[26] The geometries of all the reactants, products, various intermediates, and transition states for the $^1CHF+N_2O$ reaction are optimized using hybrid density functional B3LYP method with the 6-31G(d,p) basis set. Vibrational frequencies are calculated at the B3LYP/6-31G(d,p) level to check whether the obtained stationary point is an isomer or a first-order transition

* Author to whom correspondence should be addressed.

10.1021/jp014161g CCC: $22.00 
Published on Web 02/16/2002

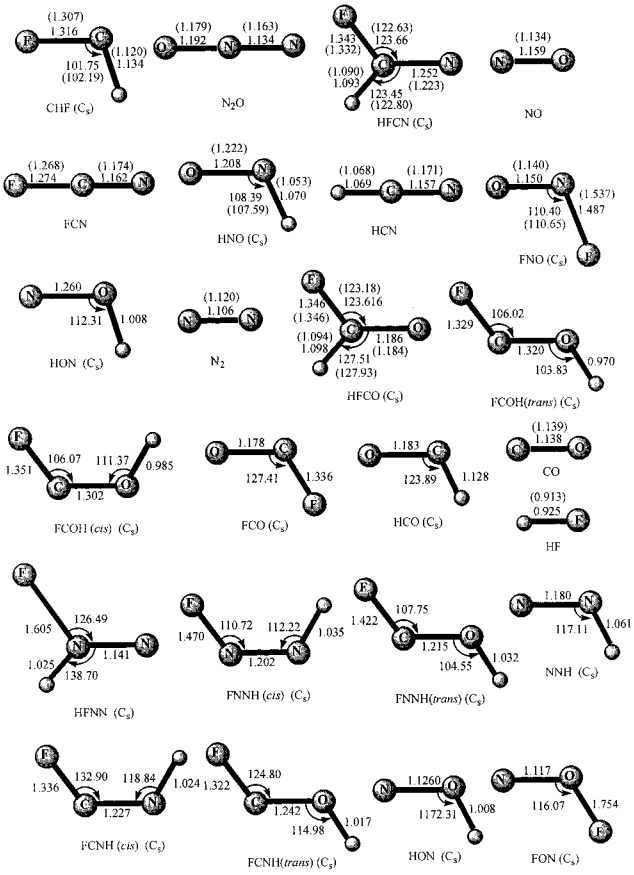


**Figure 1.** The B3LYP/6-31G(d,p)-optimized geometries of reactants and products. Bond distances are in angstroms and angles are in degrees. For the stationary points of the relevant reaction pathways, the MP2/6-311G(d,p)-calculated values are given in parentheses.

state. To confirm that the transition state connects designated intermediates, we also perform intrinsic reaction coordinate (IRC) calculations at the B3LYP/6-31G(d,p) level. In addition, single-point energies are calculated for the B3LYP/6-31G(d,p) optimized geometries with the quadratic configuration interaction method with single and double excitation and perturbative corrections for triple excitations (QCISD(T)) with the 6-311G-(d,p) basis set. Unless otherwise specified, the QCISD(T) single-point energies are used in the following discussions.

Further, to compare with DFT calculated results, we reoptimize the stationary points of the most relevant reaction pathways using the non-DFT MP2 method with the enlarged basis set of 6-311G(d,p). At the MP2 geometries, the singlet-point energies are calculated at the QCISD(T)/6-311G(2df,p) level. Unless otherwise specified, the QCISD(T)/6-311G(2df,p) single-point energies with inclusion of MP2/6-311G(d,p) zero-point energies (ZPE) are used in the following discussion.

## 3. Results and Discussions

**3.1. Isomerization and Dissociation Pathways.** Starting from the reactants **R** $^1CHF+N_2O$, twelve energetically accessible primary products (**$P_1$**−**$P_{15}$**) of the title reaction are considered in this paper. In addition, four secondary dissociation products **$P_{16}$**−**$P_{19}$** from the relevant primary products **$P_1$**, **$P_2$**, **$P_3$**, and **$P_4$** also are included. Figure 1 shows the optimized geometries of the reactants and products. The energetic data of the reactants and all products are listed in Table 1. For the present $^1CHF+N_2O$ reaction, twenty-eight intermediate isomers (denoted by the letters from **a** to **o**) including twenty-four open-chain (chainlike or branched-chain) and four cyclic species are located. Sixty-four transition states (**TS**) are obtained to connect various intermediates or products. The optimized structures of the intermediates and transition states are shown in Figures 2 and 3. Tables 2 and 3 list the energies of the intermediates and transition states, respectively. The reaction pathways related to the singlet [$CHFN_2O$] potential energy surface (PES) are schematically plotted in Figure 4, parts a and b. Note that the above-mentioned calculations are carried out at the QCISD(T)/6-311G(d,p)//B3LYP/6-31G(d,p) level. To compare with DFT-calculated results and obtain more reliable energy values, the stationary points of the most relevant reaction pathways are recalculated at the QCISD(T)/6-311G(2df,p)//MP2/6-311G(d,p) level and then the corresponding energetic data and potential energy surfaces are presented in Table 4 and Figure 4c, respectively.

The attack of the singlet CHF at the $N_2O$ molecule may have five possible ways, i.e., end-N attack, end-O attack, middle-N attack, side N−N $\pi$ bonding attack, and side N−O $\pi$ bonding attack. The end-N attack can form the chainlike isomer $HFCN_2O$ **a** (**$a_1$**, **$a_2$**, **$a_3$**). Only the addition transition state **$TSRa_1$** which links the reactants **R** to **$a_1$** can be located. In **$TSRa_1$**, the forming C−N bond is 1.610 Å, which shows the character of the "late"

**TABLE 1: Zero-Point, Total (a.u.), and Relative Energies in Parentheses (kcal/mol) as well as Those Including Zero-Point Vibration Energies (kcal/mol) of Reactants and Products for the $^1CHF+N_2O$ Reaction at the QCISD(T)/6-311G(d,p)//B3LYP/6-31G(d,p) Level**

| species | ZPE | B3LYP | QCISD(T) | QCISD(T) +ZPE |
|---|---|---|---|---|
| **R** $^1CHF+N_2O$ | 0.023517 | −323.061604 (0.0) | −322.439530 (0.0) | 0.0 |
| **$P_1$** HFCN+NO | 0.024366 | −323.100935 (−24.7) | −322.476588 (−23.3) | −22.7 |
| **$P_2$** HCN+FNO | 0.024042 | −323.127097 (−41.1) | −322.509754 (−44.1) | −43.7 |
| **$P_3$** FCN+HNO | 0.023933 | −323.101628 (−25.1) | −322.485247 (−28.7) | −28.4 |
| **$P_4$** $N_2$+HFCO | 0.026644 | −323.288454 (−142.4) | −322.676589 (−148.8) | −146.8 |
| **$P_5$** $N_2$+HOCF (c) | 0.025886 | −323.215156 (−96.4) | −322.607813 (−105.6) | −104.1 |
| **$P_6$** $N_2$+HOCF (t) | 0.025257 | −323.215444 (−96.5) | −322.606252 (−104.6) | −103.5 |
| **$P_7$** CO+HFNN | 0.024711 | −323.136326 (−46.9) | −322.524482 (−53.3) | −52.6 |
| **$P_8$** CO+HNNF(c) | 0.024882 | −323.155403 (−58.9) | −322.541802 (−64.2) | −63.3 |
| **$P_9$** CO+HNNF(t) | 0.025317 | −323.151299 (−56.3) | −322.538251 (−61.9) | −60.8 |
| **$P_{10}$** CO+$N_2$+HF | 0.019937 | −323.261045 (−125.2) | −322.678817 (−150.2) | −152.4 |
| **$P_{11}$** FCO+$N_2$H | 0.021513 | −323.127481 (−41.3) | −322.500956 (−38.5) | −39.8 |
| **$P_{12}$** NO+FCNH(c) | 0.023892 | −323.085403 (−14.9) | −322.460971 (−13.5) | −13.2 |
| **$P_{13}$** NO+FCNH(t) | 0.024744 | −323.095391 (−21.2) | −322.471090 (−19.8) | −19.0 |
| **$P_{14}$** FCN+$^1$HON | 0.023286 | −323.036475 (15.8) | −322.415828 (14.9) | 14.7 |
| **$P_{15}$** HCN+$^1$FON | 0.023612 | −323.057603 (2.5) | −322.449958 (−6.5) | −6.5 |
| **$P_{16}$** F+HCN+NO | 0.021001 | −323.028268 (20.9) | −322.428269 (7.1) | 5.5 |
| **$P_{17}$** H+FCN+NO | 0.014627 | −323.019379 (26.5) | −322.409237 (19.0) | 13.4 |
| **$P_{18}$** F+$N_2$+HCO | 0.018647 | −323.091490 (−18.9) | −322.493604 (−33.9) | −37.0 |
| **$P_{19}$** H+$N_2$+FCO | 0.013864 | −323.119157 (−36.1) | −322.512862 (−46.0) | −52.1 |

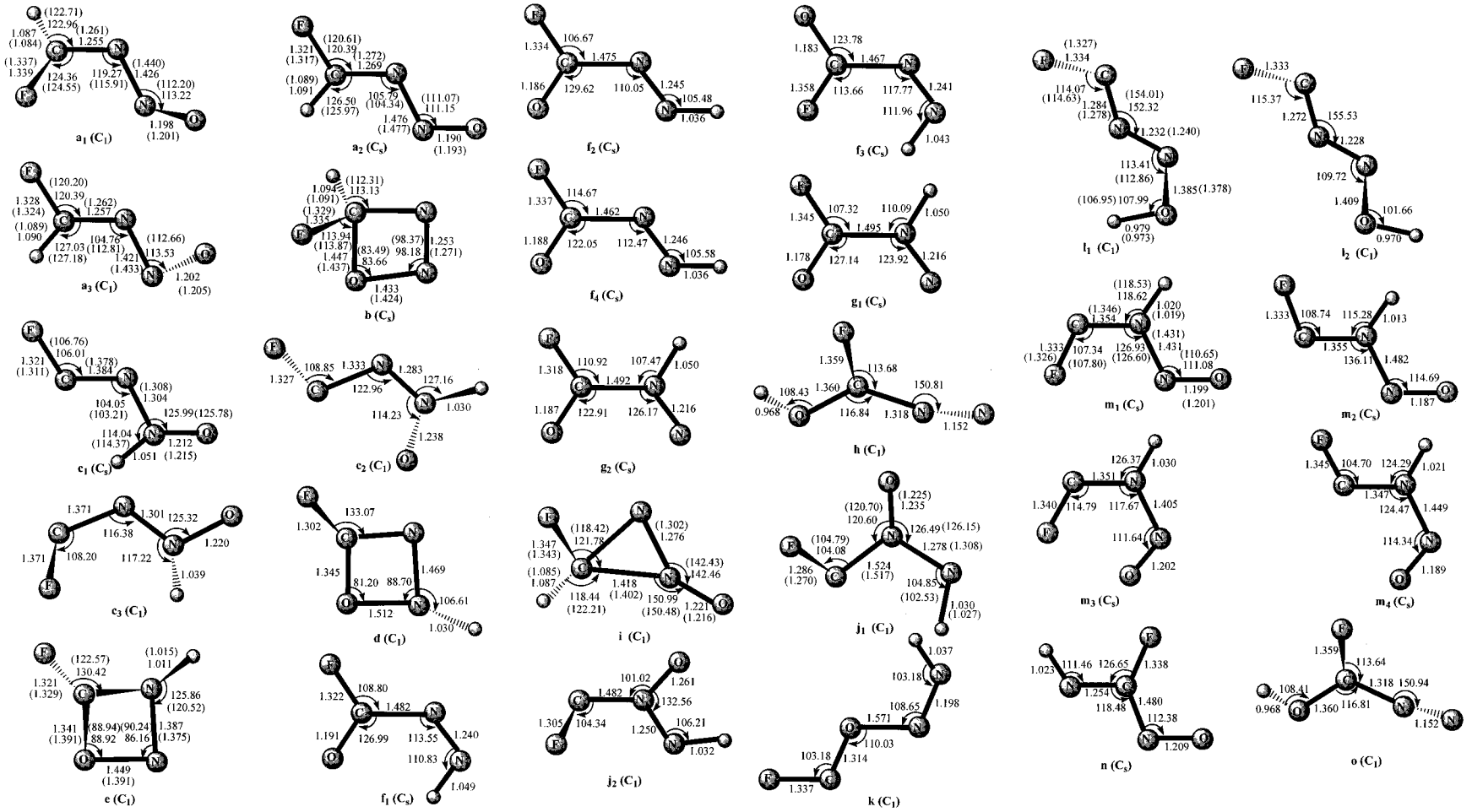


**Figure 2.** The B3LYP/6-31G(d,p)-optimized geometries of all isomers. Bond distances are in angstroms and angles are in degrees. For the stationary points of the relevant reaction pathways, the MP2/6-311G(d,p)-calculated values are given in parentheses.

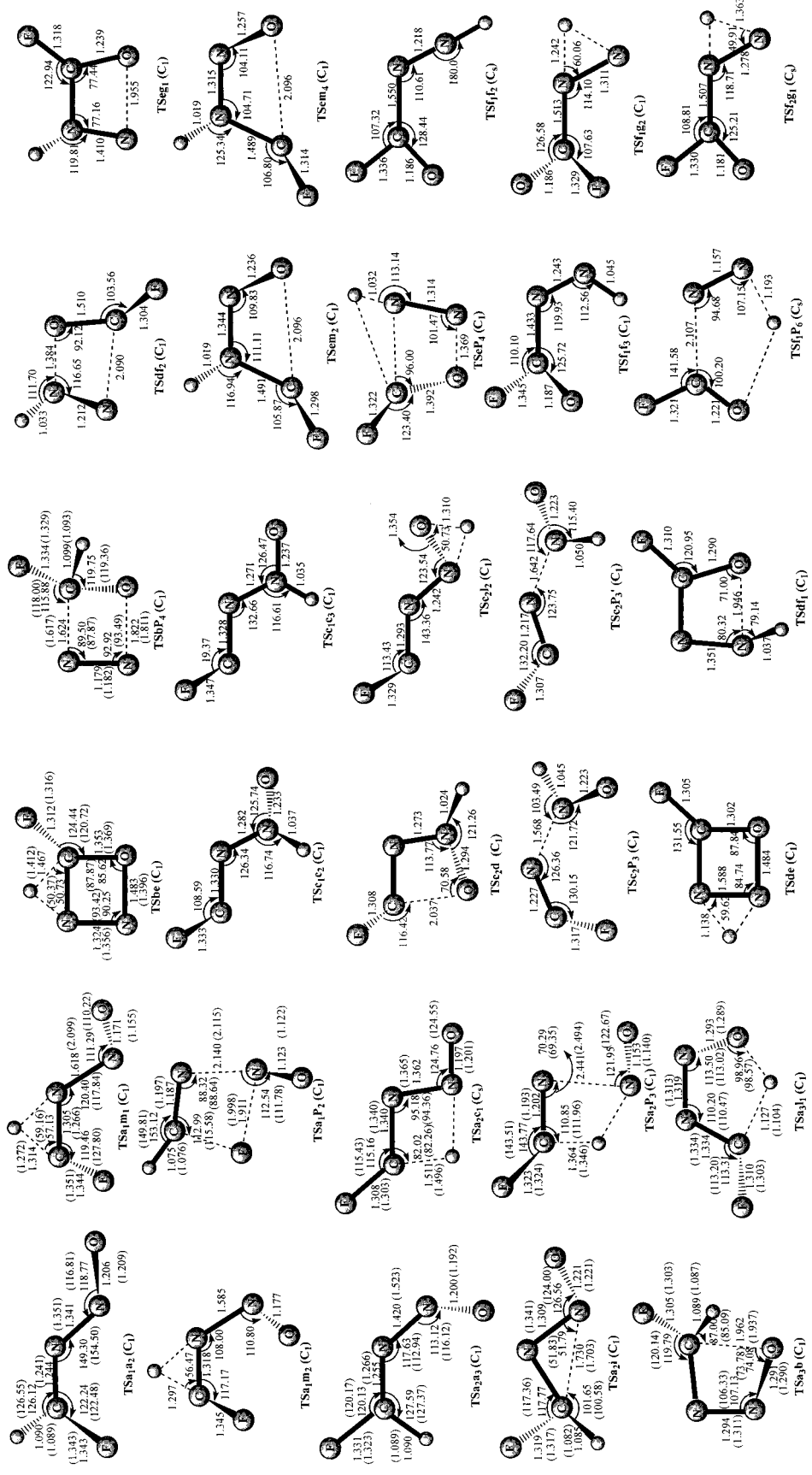
TSa$_1$a$_2$ ($C_1$)
TSa$_1$m$_2$ ($C_1$)
TSa$_2$a$_3$ ($C_1$)
TSa$_2$ ($C_1$)
TSa$_3$b ($C_1$)
TSa$_1$m$_1$ ($C_1$)
TSa$_1$P$_2$ ($C_1$)
TSa$_2$c$_1$ ($C_s$)
TSa$_2$P$_3$ ($C_1$)
TSa$_3$j$_1$ ($C_1$)
TSbe ($C_1$)
TSc$_1$c$_3$ ($C_1$)
TSc$_2$d ($C_1$)
TSc$_2$P$_3$' ($C_1$)
TSde ($C_1$)
TSbP$_4$ ($C_1$)
TSc$_2$j$_2$ ($C_1$)
TSdf$_1$ ($C_1$)
TSdf$_2$ ($C_1$)
TSem$_2$ ($C_1$)
TSef$_4$ ($C_1$)
TSf$_1$f$_5$ ($C_1$)
TSf$_1$P$_6$ ($C_s$)
TSeg$_1$ ($C_1$)
TSem$_4$ ($C_1$)
TSf$_1$f$_2$ ($C_s$)
TSf$_1$g$_2$ ($C_1$)
TSf$_2$g$_1$ ($C_s$)

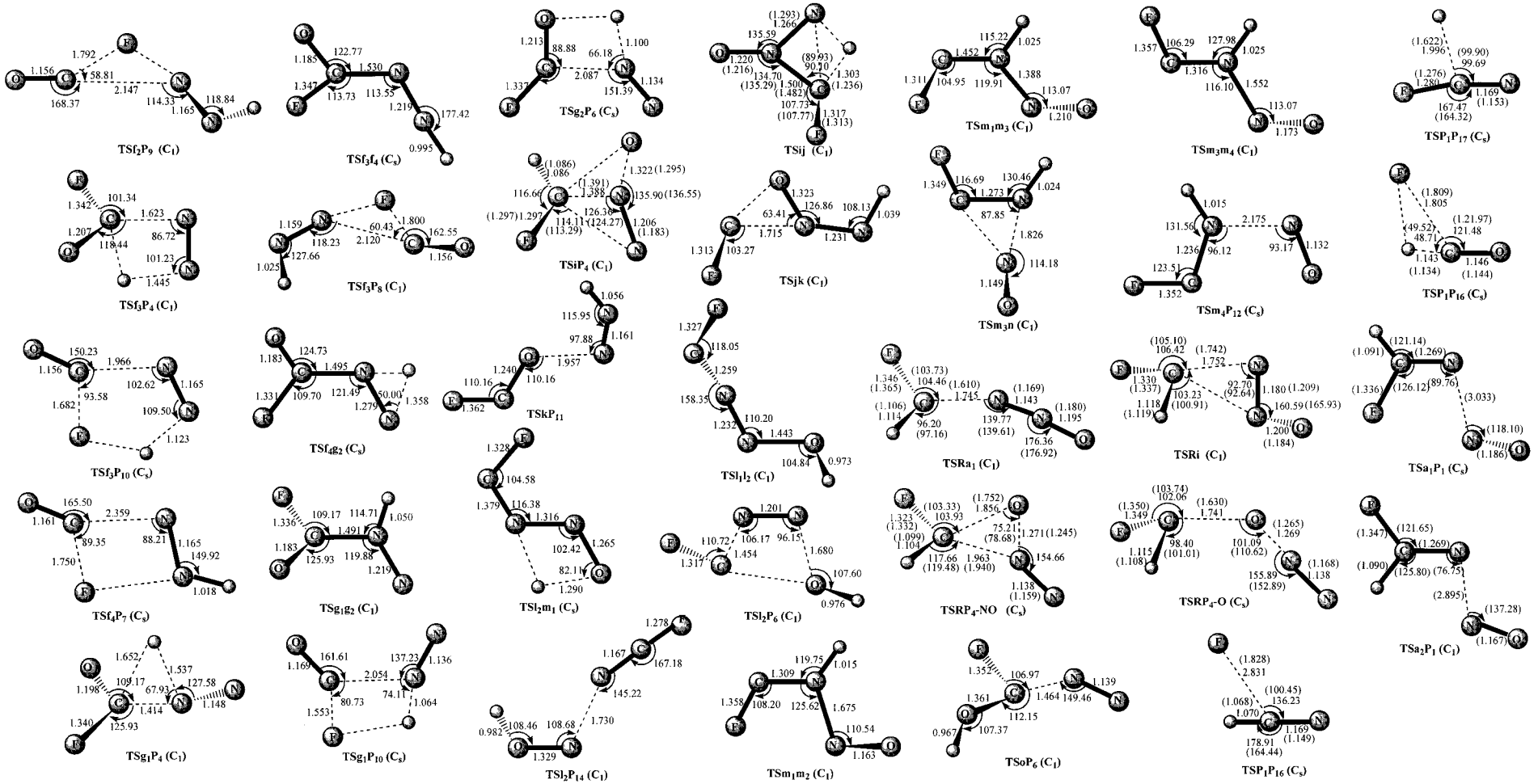


**Figure 3.** The B3LYP/6-31G(d,p)-optimized geometries of all transition states. Bond distances are in angstroms and angles are in degrees. For the stationary points of the relevant reaction pathways, the MP2/6-311G(d,p)-calculated values are given in parentheses.

**TABLE 2: Total (a.u.), and Relative Energies in Parentheses (kcal/mol) as well as Those Including Zero-Point Vibration Energies (kcal/mol) of the Intermediates for the $^1CHF+N_2O$ Reaction at the QCISD(T)/6-311g(D,P)//B3LYP/6-31G(d,p) Level**

| species | ZPE | B3LYP | QCISD(T) | QCISD(T)+ ZPE |
|---|---|---|---|---|
| $\mathbf{a_1}$ | 0.029461 | −323.149676 (−55.3) | −322.517373 (−48.8) | −45.1 |
| $\mathbf{a_2}$ | 0.029484 | −323.150745 (−55.9) | −322.519669 (−50.3) | −46.5 |
| $\mathbf{a_3}$ | 0.029412 | −323.147960 (−54.2) | −322.516274 (−48.2) | −44.5 |
| **b** | 0.031448 | −323.145827 (−52.9) | −322.515636 (−47.8) | −49.0 |
| $\mathbf{c_1}$ | 0.030144 | −323.082110 (−12.9) | −322.447512 (−5.0) | −1.0 |
| $\mathbf{c_2}$ | 0.029970 | −323.078502 (−10.6) | −322.440587 (−0.7) | 3.4 |
| $\mathbf{c_3}$ | 0.029555 | −323.067024 (−3.4) | −322.430879 (5.4) | 9.2 |
| **d** | 0.032112 | −323.134613 (−45.8) | −322.500782 (−38.4) | −33.0 |
| **e** | 0.030401 | −323.093593 (−20.1) | −322.457156 (−11.1) | −6.7 |
| $\mathbf{f_1}$ | 0.030875 | −323.207465 (−91.5) | −322.579863 (−88.1) | −83.4 |
| $\mathbf{f_2}$ | 0.030792 | −323.206672 (−91.0) | −322.580345 (−88.4) | −83.8 |
| $\mathbf{f_3}$ | 0.030640 | −323.203569 (−89.1) | −322.575014 (−85.0) | −80.5 |
| $\mathbf{f_4}$ | 0.030815 | −323.207832 (−91.8) | −322.580370 (−88.4) | −83.8 |
| $\mathbf{g_1}$ | 0.029873 | −323.173535 (−70.2) | −322.541268 (−63.8) | −59.9 |
| $\mathbf{g_2}$ | 0.030165 | −323.176315 (−72.0) | −322.543161 (−65.0) | −60.9 |
| **h** | 0.029562 | −323.163221 (−63.8) | −322.530474 (−57.1) | −53.3 |
| **i** | 0.031256 | −323.115484 (−33.8) | −322.480025 (−25.4) | −20.6 |
| $\mathbf{j_1}$ | 0.029046 | −323.048853 (8.0) | −322.417433 (13.9) | 17.3 |
| $\mathbf{j_2}$ | 0.028978 | −323.058041 (2.2) | −322.424202 (9.6) | 13.0 |
| **k** | 0.027537 | −323.104500 (−26.9) | −322.476047 (−22.9) | −20.4 |
| $\mathbf{l_1}$ | 0.028476 | −323.090195 (−17.9) | −322.453010 (−8.5) | −5.3 |
| $\mathbf{l_2}$ | 0.028820 | −323.094336 (−20.5) | −322.457706 (−11.4) | −8.1 |
| $\mathbf{m_1}$ | 0.028829 | −323.103955 (−26.6) | −322.473904 (−21.6) | −18.2 |
| $\mathbf{m_2}$ | 0.028426 | −323.097557 (−22.6) | −322.467533 (−17.6) | −14.5 |
| $\mathbf{m_3}$ | 0.028740 | −323.105806 (−27.7) | −322.476166 (−23.0) | −19.7 |
| $\mathbf{m_4}$ | 0.028322 | −323.098980 (−23.5) | −322.470086 (−19.2) | −16.2 |
| **n** | 0.030062 | −323.157197 (−60.0) | −322.527837 (−55.4) | −51.3 |
| **o** | 0.029559 | −323.163222 (−63.8) | −322.530503 (−57.1) | −53.3 |

transition state. Therefore, $\mathbf{TSRa_1}$ lies 13.5 kcal/mol higher than the reactants **R**. Note that the transition states $\mathbf{TSRa_2}$ and $\mathbf{TSRa_3}$ cannot be obtained. However, as shown in Figure 4 c, $\mathbf{a_1}$ can isomerize to $\mathbf{a_2}$ after surmounting the barrier of 15.4 kcal/mol, and then $\mathbf{a_2}$ can convert easily to $\mathbf{a_3}$. Both end-O and side N−O $\pi$ bonding attacks directly lead to the same product $\mathbf{P_4}$ $N_2$+HFCO via the transition states $\mathbf{TSRP_4\text{-}O}$ and $\mathbf{TSRP_4\text{-}NO}$, which lie 18.7 and 21.0 kcal/mol above the reactants **R**, respectively. Clearly, these two attacks are considerably barrier-consumed processes. The other barrier-consumed process is a side N−N $\pi$ bonding attack leading to the three-membered ring isomer HF-c(CNN)O **i**. The transition state **TSRi** is 20.1 kcal/mol higher than the reactants **R**. As shown in Figure 4c, **i** is readily isomerized to end-N adduct $\mathbf{a_2}$ through the ring-open transition state $\mathbf{TSa_2i}$. Such a process requires only overcoming 18.8 kcal/mol barrier relative to **i**. Therefore, the formation of **i** is not likely important for the total reaction. We try to optimize the adduct of middle-N attack, yet with no success. Such a search usually leads to **a** or **i**. By comparison, we can find that the end-N attack is energetically the most feasible way. In the following discussions, we mainly discuss the formation pathways of various products formed via **a**.

Starting from $HFCN_2O$ **a**, various products can be formed via successive isomerization and dissociation pathways. In the following parts, we will first discuss the formation pathways of the four kinetically feasible products $\mathbf{P_1}$ HFCN+NO, $\mathbf{P_2}$ HCN+FNO, $\mathbf{P_3}$ FCN+HNO, and $\mathbf{P_4}$ $N_2$+HFCO.

*3.1.1.* $\mathbf{P_1}$ *HFCN+NO,* $\mathbf{P_2}$ *HCN+FNO,* $\mathbf{P_3}$ *FCN+HNO, and* $\mathbf{P_4}$ $N_2$*+HFCO.* The initially formed end-N attack isomer $HFCN_2O$ **a** can directly dissociate to the product $\mathbf{P_1}$ HFCN+NO via the N−N single bond rupture. Such a simple process can be depicted as:

**Path1 $\mathbf{P_1}$:** **R** $^1CHF+N_2O \rightarrow$ *trans*-$HFCN_2O$ $\mathbf{a_1} \rightarrow$ $\mathbf{P_1}$ HFCN+NO

**Path2 $\mathbf{P_1}$:** **R** $^1CHF+N_2O \rightarrow$ *trans*-$HFCN_2O$ $\mathbf{a_1} \rightarrow$ *trans*-$HFCN_2O$ $\mathbf{a_2} \rightarrow \mathbf{P_1}$ HFCN+NO

Despite numerous attempts, optimization of any transition structures from **a** to $\mathbf{P_1}$ often leads to product $\mathbf{P_1}$ or **a** at the B3LYP/6-31G(d,p) level. At the MP2/6-311G(d,p) level, the transition states $\mathbf{TSa_2P_1}$ and $\mathbf{TSa_1P_1}$ are obtained. However, single-point energy calculations show that $\mathbf{TSa_2P_1}$ and $\mathbf{TSa_1P_1}$ lie 3.3 and 3.5 kcal/mol lower than $\mathbf{P_1}$, respectively. It indicates that after surmounting the barriers of $\mathbf{TSa_2P_1}$ and $\mathbf{TSa_1P_1}$, the very stable complexes might be formed followed by the dissociation to $\mathbf{P_1}$.

The isomer *trans*-$HFCN_2O$ $\mathbf{a_1}$ can alternatively undergo a concerted F-shift and N−N bond rupture leading to product $\mathbf{P_2}$ HCN+FNO. Similarly, *trans*-$HFCN_2O$ $\mathbf{a_2}$ can also undergo a concerted H-shift and N−N bond cleavage to form product $\mathbf{P_3}$ FCN+HNO via $\mathbf{TSa_2P_3}$. It should be pointed out that the transition states $\mathbf{TSa_2P_3}$ could be obtained only using B3LYP method. At the MP2/6-311G(d,p) level, optimization of such a transition state always leads to two separated fragments. The isomer *cis*-$CHFN_2O$ $\mathbf{a_3}$ can take a ring-closure to form the four-membered ring intermediate HF-c(CNNO) **b** followed by dissociation to product $\mathbf{P_4}$ $N_2$+HFCO. These product channels can be written as:

**Path $\mathbf{P_2}$:** **R** $^1CHF+N_2O \rightarrow$ *trans*-$HFCN_2O$ $\mathbf{a_1} \rightarrow$ $\mathbf{P_2}$ HCN+FNO

**Path $\mathbf{P_3}$:** **R** $^1CHF+N_2O \rightarrow$ *trans*-$HFCN_2O$ $\mathbf{a_1} \rightarrow$ *trans*-$HFCN_2O$ $\mathbf{a_2} \rightarrow \mathbf{P_3}$ FCN+HNO

**Path $\mathbf{P_4}$:** **R** $^1CHF+N_2O \rightarrow$ *trans*-$HFCN_2O$ $\mathbf{a_1} \rightarrow$ *cis*-$HFCN_2O$ $\mathbf{a_3} \rightarrow$ HF-c(CNNO) **b** $\rightarrow \mathbf{P_4}$ $N_2$+HFCO

Note that the interconversion between $\mathbf{a_2}$ and $\mathbf{a_3}$ takes place easily and thus, for simplicity, these processes are not shown.

Subsequently, let us discuss the secondary dissociation reactions of the feasible products $\mathbf{P_1}$ HFCN+NO, $\mathbf{P_2}$ HCN+FNO, $\mathbf{P_3}$ FCN+HNO, and $\mathbf{P_4}$ $N_2$+HFCO. Products $\mathbf{P_1}$, $\mathbf{P_2}$, and $\mathbf{P_3}$ can further dissociate to give $\mathbf{P_{16}}$ F+HCN+NO or $\mathbf{P_{17}}$ H+FCN+NO via the direct C(N)−H or C(N)−F bond rupture.

**TABLE 3: Zero-Point, Total (a.u.), and Relative Energies in Parentheses (kcal/mol) as well as Those Including Zero-Point Vibration Energies (kcal/mol) of the Transition States for the $^1CHF+N_2O$ Reaction at the QCISD(T)/6-311G(d,p)//B3LYP/6-31G(d,p) Level**

| species | ZPE | B3LYP | QCISD(T) | QCISD(T) +ZPE |
|---|---|---|---|---|
| **$TSa_1a_2$** | 0.028753 | −323.133156 (−44.9) | −322.490772 (−32.2) | −28.9 |
| **$TSa_1m_1$** | 0.021648 | −323.028721 (20.6) | −322.397081 (26.6) | 25.5 |
| **$TSa_1m_2$** | 0.021946 | −323.026592 (22.0) | −322.396264 (27.1) | 26.2 |
| **$TSa_1P_2$** | 0.026245 | −323.090249 (−18.0) | −322.461914 (−14.0) | −12.3 |
| **$TSa_2a_3$** | 0.029123 | −323.147908 (−54.2) | −322.516034 (−48.0) | −44.5 |
| **$TSa_2c_1$** | 0.025688 | −323.064756 (−2.0) | −322.427917 (7.3) | 8.6 |
| **$TSa_2i$** | 0.029033 | −323.085850 (−15.2) | −322.448480 (−5.6) | −2.2 |
| **$TSa_2P_3$** | 0.022528 | −323.069363 (−4.9) | −322.441355 (−1.1) | −1.8 |
| **$TSa_3b$** | 0.029737 | −323.108624 (−29.5) | −322.472579 (−20.7) | −16.8 |
| **$TSa_3l_1$** | 0.025458 | −323.072314 (−6.7) | −322.434535 (3.1) | 4.4 |
| **TSbe** | 0.025813 | −323.046283 (9.6) | −322.410318 (18.3) | 19.8 |
| **$TSbP_4$** | 0.028658 | −323.122397 (−38.1) | −322.491461 (−32.6) | −29.4 |
| **$TSc_1c_2$** | 0.029046 | −323.071753 (−6.4) | −322.433622 (3.7) | 7.2 |
| **$TSc_1c_3$** | 0.029019 | −323.061913 (−0.2) | −322.422433 (10.7) | 14.2 |
| **$TSc_2d$** | 0.029312 | −323.060508 (0.7) | −322.422808 (10.5) | 14.1 |
| **$TSc_2l_2$** | 0.022592 | −322.996095 (41.1) | −322.354152 (53.6) | 53.0 |
| **$TSc_2P_3$** | 0.027215 | −323.049519 (7.6) | −322.415446 (15.1) | 17.4 |
| **$TSc_2P_3'$** | 0.027131 | −323.042731 (11.8) | −322.408811 (19.3) | 21.5 |
| **TSde** | 0.026333 | −323.051500 (6.3) | −322.415761 (14.9) | 16.7 |
| **$TSdf_1$** | 0.029742 | −323.110638 (30.8) | −322.476389 (−23.1) | −19.2 |
| **$TSdf_2$** | 0.027491 | −323.031190 (19.1) | −322.396239 (27.2) | 29.7 |
| **$TSem_2$** | 0.027489 | −323.059904 (1.1) | −322.428290 (7.1) | 9.5 |
| **$TSem_4$** | 0.028263 | −323.065110 (1.1) | −322.430620 (5.6) | 8.6 |
| **$TSeg_1$** | 0.028570 | −323.075221 (−8.5) | −322.437545 (1.2) | 4.4 |
| **$TSeP_4$** | 0.027596 | −323.031366 (19.0) | −322.400029 (24.8) | 27.3 |
| **$TSf_1f_2$** | 0.027758 | −323.132152 (−44.3) | −322.499484 (−37.6) | −35.0 |
| **$TSf_1f_3$** | 0.030263 | −323.200503 (−87.2) | −322.572329 (−83.3) | −79.1 |
| **$TSf_1f_5$** | 0.027780 | −323.132151 (−44.3) | −322.499483 (−37.6) | −34.9 |
| **$TSf_1g_2$** | 0.023443 | −323.051431 (6.4) | −322.421005 (−11.6) | −3.1 |
| **$TSf_1P_6$** | 0.025322 | −323.163843 (−64.2) | −322.533188 (−53.8) | −57.6 |
| **$TSf_2g_1$** | 0.024481 | −323.091594 (−18.8) | −322.463283 (−14.9) | −14.3 |
| **$TSf_2P_9$** | 0.024415 | −323.080557 (−11.9) | −322.447146 (−4.8) | −4.2 |
| **$TSf_3f_4$** | 0.027744 | −323.131878 (−44.1) | −322.498565 (−37.0) | −34.4 |
| **$TSf_3P_4$** | 0.024523 | −323.093898 (−20.3) | −322.463002 (−14.7) | −14.1 |
| **$TSf_3P_8$** | 0.025033 | −323.096690 (−22.0) | −322.466871 (−17.2) | −16.2 |
| **$TSf_3P_{10}$** | 0.025247 | −323.155469 (−58.9) | −322.526112 (−54.3) | −53.2 |
| **$TSf_4g_2$** | 0.024611 | −323.092247 (−20.3) | −322.462998 (−14.7) | −14.0 |
| **$TSf_4P_7$** | 0.024525 | −323.095929 (−21.5) | −322.471281 (−19.9) | −19.3 |
| **$TSg_1g_2$** | 0.029236 | −323.163221 (−63.8) | −322.531244 (−57.6) | −54.0 |
| **$TSg_1P_4$** | 0.024204 | −323.103639 (−26.4) | −322.470928 (−19.7) | −19.3 |
| **$TSg_1P_{10}$** | 0.025745 | −323.140958 (−49.8) | −322.509418 (−43.9) | −42.5 |
| **$TSg_2P_6$** | 0.025762 | −323.143327 (−51.3) | −322.511921 (−45.4) | −44.0 |
| **TSij** | 0.025224 | −323.024528 (23.3) | −322.392305 (29.6) | 30.7 |
| **$TSiP_4$** | 0.028028 | −323.034815 (16.8) | −322.405260 (21.5) | 24.3 |
| **TSjk** | 0.027423 | −323.045327 (10.2) | −322.410723 (18.1) | 20.5 |
| **$TSkP_{11}$** | 0.025107 | −323.099989 (−24.1) | −322.468872 (−18.4) | −17.4 |
| **$TSl_1l_2$** | 0.027326 | −323.080434 (−11.8) | −322.445026 (−3.4) | −1.1 |
| **$TSl_2m_1$** | 0.024266 | −323.044879 (10.5) | −322.410623 (18.1) | 18.6 |
| **$TSl_2P_6$** | 0.026364 | −323.064593 (−1.9) | −322.431315 (5.2) | 6.9 |
| **$TSl_2P_{14}$** | 0.026136 | −323.022412 (24.6) | −322.386880 (33.0) | 34.7 |
| **$TSm_1m_2$** | 0.026799 | −323.086278 (−15.5) | −322.458956 (−12.2) | −9.9 |
| **$TSm_1m_3$** | 0.026563 | −323.058052 (2.2) | −322.426462 (8.2) | 10.1 |
| **$TSm_3m_4$** | 0.026729 | −323.081916 (−12.7) | −322.457425 (−11.2) | −9.2 |
| **$TSm_3n$** | 0.026633 | −323.079163 (−11.0) | −322.445468 (−3.7) | −1.8 |
| **$TSm_4P_{12}$** | 0.027057 | −323.075941 (−9.0) | −322.449915 (−6.5) | −4.3 |
| **$TSRa_3$** | 0.026498 | −323.056351 (3.5) | −322.421334 (11.4) | 13.2 |
| **TSRi** | 0.026523 | −323.044198 (10.9) | −322.407903 (19.8) | 21.7 |
| **$TSRP_4$-O** | 0.025968 | −323.045078 (10.4) | −322.410239 (18.4) | 19.9 |
| **$TSRP_4$-NO** | 0.026778 | −323.042583 (11.9) | −322.406421 (20.8) | 22.8 |
| **$TSoP_6$** | 0.027921 | −323.161215 (−62.5) | −322.532479 (−58.3) | −55.6 |
| **$TSP_1P_{16}$** | 0.021296 | −323.031222 (19.1) | −322.427812 (7.4) | 6.0 |
| **$TSP_1P_{17}$** | 0.015537 | −323.016103 (28.5) | −322.400468 (24.5) | 19.5 |
| **$TSP_4P_{10}$** | 0.020969 | −323.199924 (−86.8) | −322.589845 (−94.3) | −95.9 |
| [a] **$TSa_1P_1$** | 0.032856 | −323.252653 | −322.485979 (−29.1) | −23.3 |
| [a] **$TSa_2P_1$** | 0.026218 | −323.272216 | −322.477739 (−24.0) | −22.3 |

[a] The calculated results at the MP2/6-31G(d,p) level.

However, both **$P_{16}$** and **$P_{17}$** are 16.1 and 17.3 kcal/mol higher than the reactants **R**. Thus, the secondary dissociation reactions of **$P_1$**, **$P_2$**, and **$P_3$** are thermodynamically prohibited. In addition, **$P_4$** also can further dissociate to form the products **$P_{10}$** $CO+N_2+HF$, **$P_{18}$** $F+N_2+HCO$, and **$P_{19}$** $H+N_2+FCO$ via the side HF-elimination, and C−F and C−H bond rupture, respectively. Yet, formation of **$P_{10}$** requires surmounting the barrier of 52.4 kcal/mol, while formation of **$P_{18}$** and **$P_{19}$** needs the

**a**

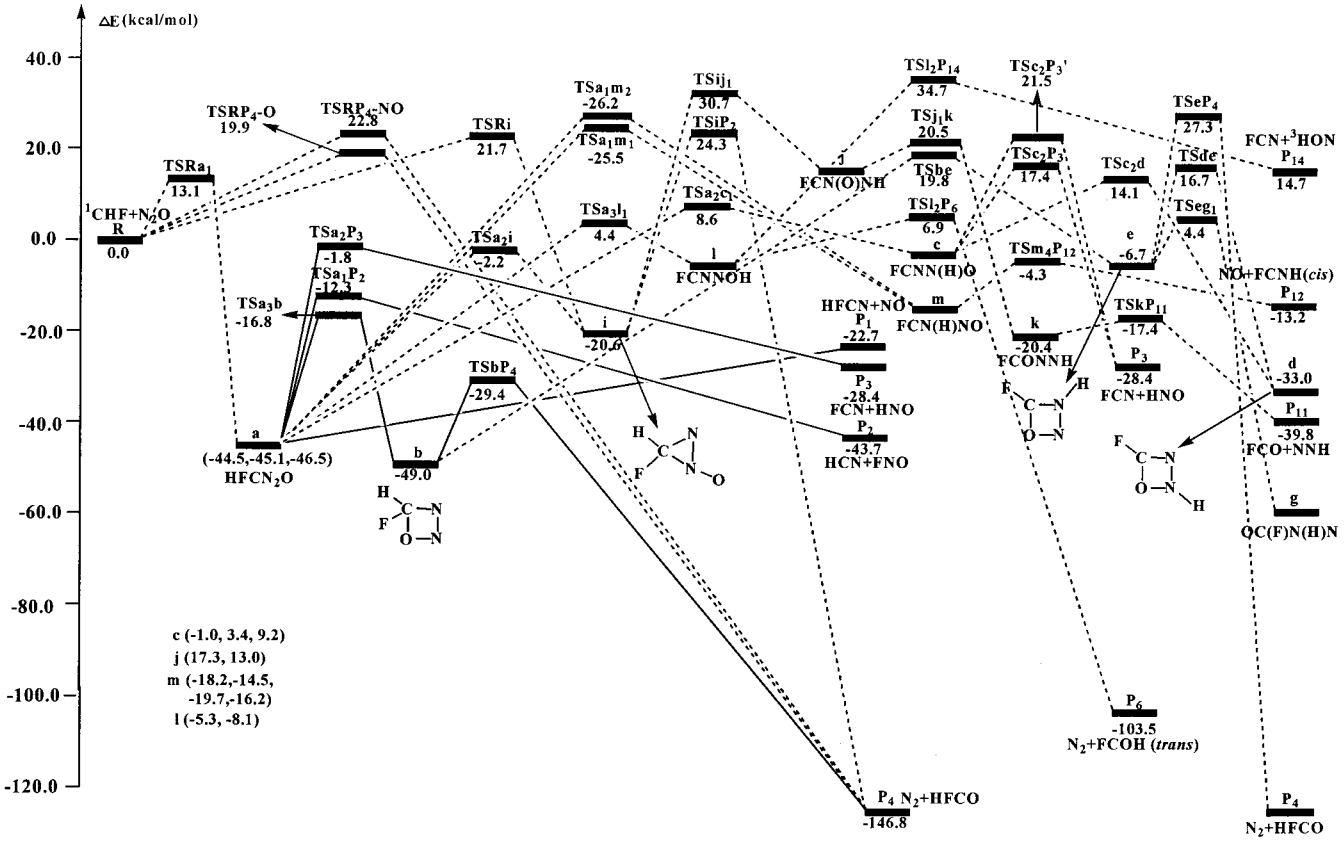
ΔE (kcal/mol)
40.0
20.0
0.0
-20.0
-40.0
-60.0
-80.0
-100.0
-120.0
$^1$CHF+N$_2$O
R
0.0
TSRa$_1$
13.1
TSRP$_4$-O
19.9
TSRP$_4$-NO
22.8
TSRi
21.7
TSa$_1$m$_2$
-26.2
TSa$_1$m$_1$
-25.5
TSij$_1$
30.7
TSiP$_2$
24.3
TSa$_2$c$_1$
8.6
TSa$_3$l$_1$
4.4
TSa$_2$P$_3$
-1.8
TSa$_1$P$_2$
-12.3
TSa$_2$i
-2.2
TSa$_3$b
-16.8
TSbP$_4$
-29.4
TSl$_2$P$_{14}$
34.7
TSj$_1$k
20.5
TSbe
19.8
TSl$_2$P$_6$
6.9
TSc$_2$P$_3$'
21.5
TSc$_2$P$_3$
17.4
TSm$_4$P$_{12}$
-4.3
TSkP$_{11}$
-17.4
TSePd
27.3
TSc$_2$d
14.1
TSde
16.7
TSeg$_1$
4.4
FCN+$^3$HON
P$_{14}$
14.7
NO+FCNH(*cis*)
P$_{12}$
-13.2
d
-33.0
P$_{11}$
-39.8
FCO+NNH
g
OC(F)N(H)N
a
(-44.5,-45.1,-46.5)
HFCN$_2$O
b
-49.0
i
-20.6
j
FCN(O)NH
l
FCNNOH
c
FCNN(H)O
m
FCN(H)NO
k
-20.4
FCONNH
e
-6.7
HFCN+NO
P$_1$
-22.7
P$_3$
-28.4
FCN+HNO
P$_2$
-43.7
HCN+FNO
P$_3$
-28.4
FCN+HNO
P$_6$
-103.5
N$_2$+FCOH (*trans*)
P$_4$ N$_2$+HFCO
-146.8
P$_4$
N$_2$+HFCO
c (-1.0, 3.4, 9.2)
j (17.3, 13.0)
m (-18.2,-14.5,
-19.7,-16.2)
l (-5.3, -8.1)

**b**

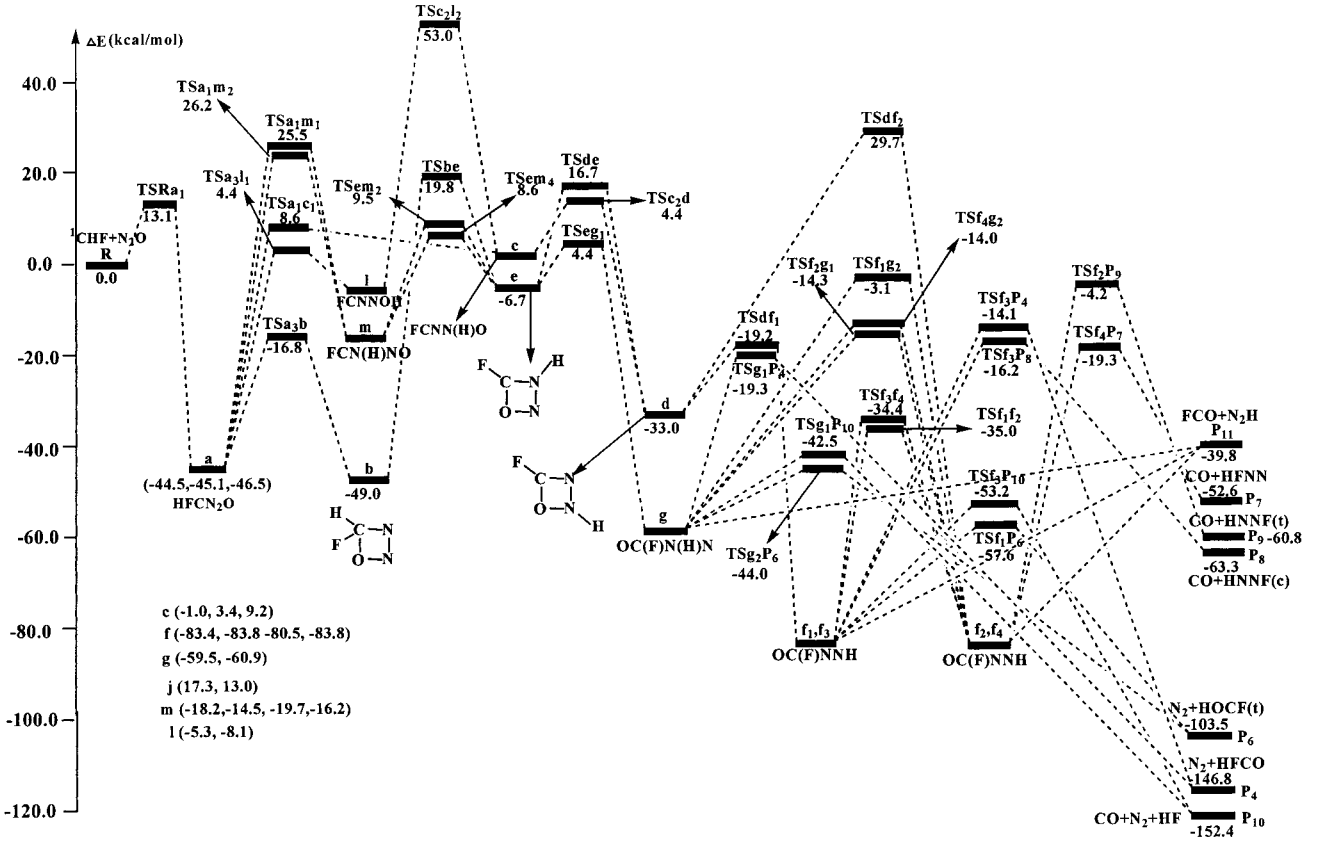
ΔE (kcal/mol)
40.0
20.0
0.0
-20.0
-40.0
-60.0
-80.0
-100.0
-120.0
$^1$CHF+N$_2$O
R
0.0
TSRa$_1$
13.1
TSc$_2$l$_2$
53.0
TSa$_1$m$_2$
26.2
TSa$_1$m$_1$
25.5
TSa$_3$l$_1$
4.4
TSa$_1$c$_1$
8.6
TSem$_2$
9.5
TSbe
19.8
TSem$_4$
8.6
TSde
16.7
TSc$_2$d
4.4
TSeg$_1$
4.4
TSa$_3$b
-16.8
TSdf$_2$
29.7
TSf$_4$g$_2$
-14.0
TSf$_2$g$_1$
-14.3
TSf$_1$g$_2$
-3.1
TSf$_2$P$_9$
-4.2
TSf$_3$P$_4$
-14.1
TSf$_4$P$_7$
-19.3
TSf$_3$P$_8$
-16.2
TSdf$_1$
-19.2
TSg$_1$P$_5$
-19.3
TSf$_3$f$_4$
-34.4
TSf$_1$f$_2$
-35.0
TSg$_1$P$_{10}$
-42.5
TSf$_3$P$_{10}$
-53.2
TSf$_1$P$_6$
-57.6
TSg$_2$P$_6$
-44.0
FCO+N$_2$H
P$_{11}$
-39.8
CO+HFNN
-52.6
P$_7$
CO+HNNF(t)
P$_9$ -60.8
P$_8$
-63.3
CO+HNNF(c)
a
(-44.5,-45.1,-46.5)
HFCN$_2$O
b
-49.0
l
FCNNOH
m
FCN(H)NO
c
FCNN(H)O
e
-6.7
d
-33.0
g
OC(F)N(H)N
f$_1$,f$_3$
OC(F)NNH
f$_2$,f$_4$
OC(F)NNH
N$_2$+HOCF(t)
-103.5
P$_6$
N$_2$+HFCO
-146.8
P$_4$
CO+N$_2$+HF
-152.4
P$_{10}$
c (-1.0, 3.4, 9.2)
f (-83.4, -83.8 -80.5, -83.8)
g (-59.5, -60.9)
j (17.3, 13.0)
m (-18.2,-14.5, -19.7,-16.2)
l (-5.3, -8.1)

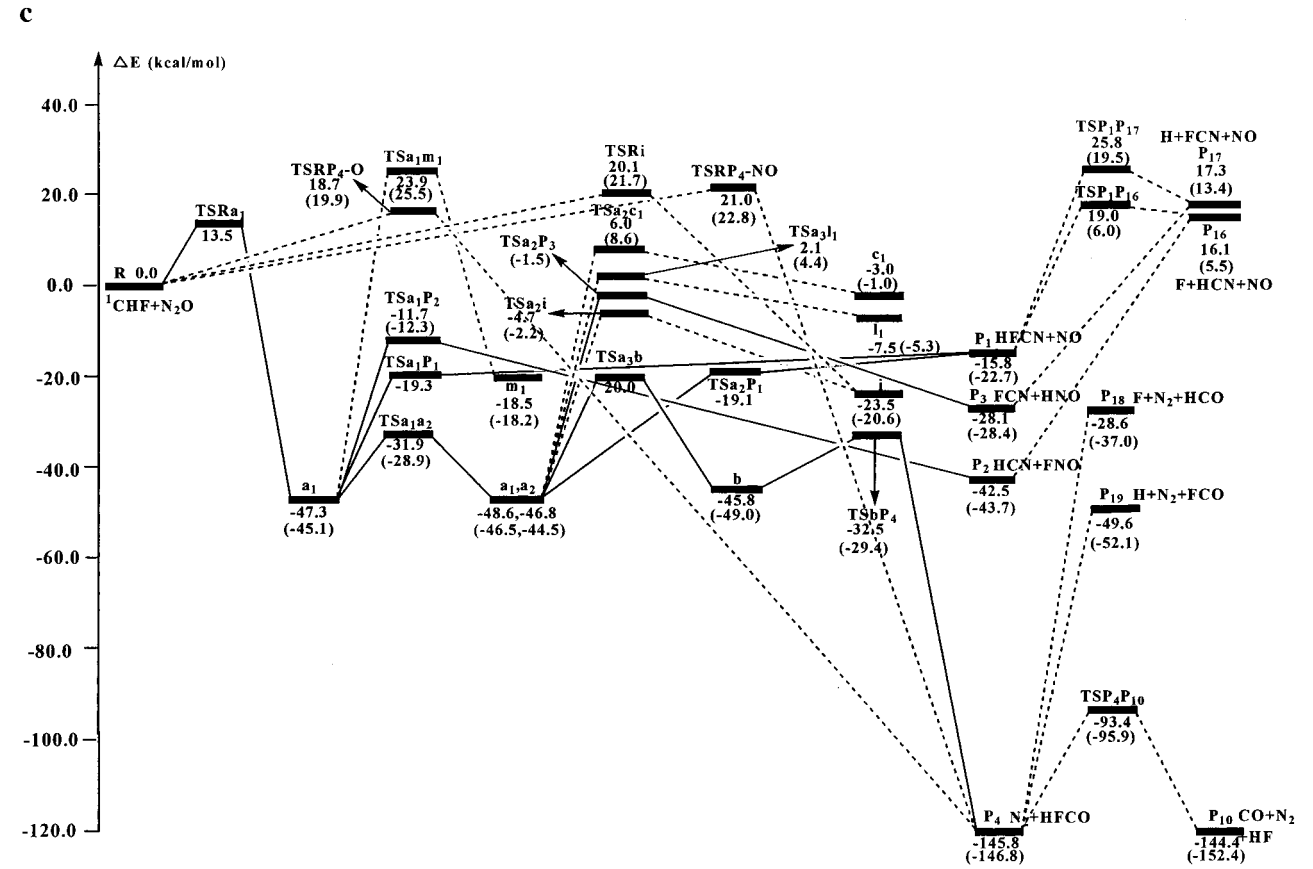


**Figure 4.** **(a)** The potential energy surface of the relevant reaction pathways for the $^1CHF+N_2O$ reaction at the QCISD(T)/6-311G(d,p)//B3LYP/6-31G(d,p)+ZPE level. **(b)** The potential energy surface of the unfavorable reaction channels for the $^1CHF+N_2O$ reaction at the QCISD(T)/6-311G(d,p)//B3LYP/6-31G(d,p)+ZPE level. **(c)** The potential energy surface of the relevant reaction pathways for the $^1CHF+N_2O$ reaction at the QCISD(T)/6-311G(2df,p)//MP2/6-311G(d,p)+ZPE level. The calculated results at the QCISD(T)/6-311G(d,p)//B3LYP/6-31G(d,p)+ZPE level are given in parentheses.

endothermicities of 117.2 and 96.2 kcal/mol, respectively. It implies that the low-lying $\mathbf{P_4}$ is kinetically stable and is not readily further dissociated.

*3.1.2. Other Products.* Finally, we turn to the other isomerization and dissociation channels of the isomers $HFCN_2O$ **a** and HF-c(CNNO) **b**. As shown in Figure 4a, the isomers $HFCN_2O$ $\mathbf{a_1}$, $\mathbf{a_2}$, and $\mathbf{a_3}$ can undergo 1,2-H-shift, 1,3-H-shift, and 1,4-H-shift leading to chainlike isomers FCN(H)NO $\mathbf{m_1}$, FCNN(H)O $\mathbf{c_1}$, and FCNNOH $\mathbf{l_1}$, respectively. However, these conversion transition states $\mathbf{TSa_1m_1}$, $\mathbf{TSa_2c_1}$, and $\mathbf{TSa_3l_1}$ lie 23.9, 6.0, and 2.1 kcal/mol above the reactants **R**. It is worthwhile noticing that $\mathbf{TSa_1m_2}$ is also obtained at the B3LYP/6-31G(d,p) level. Also, such a transition state lies 26.2 kcal/mol higher than **R** and thus this conversion process is unimportant for the total reaction. The four-membered ring isomer HF-c(CNNO) **b** can undergo 1,2-H-shift from C-atom to N-atom to give the other four-membered ring intermediate F−c(CN(H)NO) **e** via the transition state **TSbe** with the relative energy of 17.2 kcal/mol. Clearly, all these H-migration reaction pathways are not feasible for the $^1CHF+N_2O$ reaction. Therefore, though **c**, **e**, **l**, and **m** can further convert to the other isomers or the products $\mathbf{P_4}$ $N_2$+HFCO, $\mathbf{P_6}$ $N_2$+HOCF(trans), $\mathbf{P_{12}}$ NO+FCNH (cis), $\mathbf{P_{14}}$ FCN+$^1$HON, these processes are kinetically unfeasible.

It should be pointed out that the OCNN-framed isomers OC(F)NNH **f** and OC(F)N(H)N **g** are very stable, as shown in Figure 4b. However, all reaction pathways leading to them involve the high-lying transition states that lie above the reactants **R**. Although **f** and **g** can lead to the complex products $\mathbf{P_4}$ $N_2$+HFCO, $\mathbf{P_6}$ $N_2$+HOCF(trans), $\mathbf{P_7}$ CO+HFNN, $\mathbf{P_8}$ CO+HNNF(cis), $\mathbf{P_9}$ CO+HNNF(trans), $\mathbf{P_{10}}$ CO+$N_2$+HF, and $\mathbf{P_{11}}$ FCO+NNH via the various pathways among which the involved transition states are lower than the reactants **R**, formation of these products seem kinetically unfeasible for the $^1CHF+N_2O$ reaction.

**3.2. Reaction Mechanism.** In Section 3.1, we have obtained several important reaction channels that are both thermodynamically and kinetically accessible for the $^1CHF+N_2O$ reaction. Here, for easier discussions, they are listed again:

**Path1 $\mathbf{P_1}$:** **R** $^1CHF+N_2O \rightarrow$ *trans*-$HFCN_2O$ $\mathbf{a_1} \rightarrow$ $\mathbf{P_1}$ HFCN+NO

**Path2 $\mathbf{P_1}$:** **R** $^1CHF+N_2O \rightarrow$ *trans*-$HFCN_2O$ $\mathbf{a_1} \rightarrow$ *trans*-$HFCN_2O$ $\mathbf{a_2} \rightarrow$ $\mathbf{P_1}$ HFCN+NO

**Path $\mathbf{P_2}$:** **R** $^1CHF+N_2O \rightarrow$ *trans*-$HFCN_2O$ $\mathbf{a_1} \rightarrow$ $\mathbf{P_2}$ HCN+FNO

**Path $\mathbf{P_3}$:** **R** $^1CHF+N_2O \rightarrow$ *t rans*-$HFCN_2O$ $\mathbf{a_1} \rightarrow$ *trans*-$HFCN_2O$ $\mathbf{a_2} \rightarrow$ $\mathbf{P_3}$ FCN+HNO

**Path $\mathbf{P_4}$:** **R** $^1CHF+N_2O \rightarrow$ *trans*-$HFCN_2O$ $\mathbf{a_1} \rightarrow$ *cis*-$HFCN_2O$ $\mathbf{a_3} \rightarrow$ HF-c(CNNO) **b** $\rightarrow$ $\mathbf{P_4}$ $N_2$+HFCO

As shown in Figure 4c, these reaction pathways are depicted with a solid line. For these five reaction channels, the least competitive channel should be **Path $\mathbf{P_3}$** due to the high-energy

**TABLE 4: Zero-Point, Total (a.u.), and Relative Energies in Parentheses (kcal/mol) as well as Those Including Zero-Point Vibration Energies (kcal/mol) of Reactants, Products, Isomers, Transition States on the Relevant Reaction Pathways at the QCISD(T)/6-311G(2df, p)//MP2/6-311G(d,p) Level**

| species | ZPE | MP2 | QCISD(T) | QCISD(T) +ZPE |
|---|---|---|---|---|
| **R** $^1$CHF+$N_2$O | 0.023549 | −322.399021 (0.0) | −322.605800 (0.0) | 0.0 |
| **P$_1$** HFCN+NO | 0.029708 | −322.410548 (−7.2) | −322.637212 (−19.7) | −15.8 |
| **P$_2$** HCN+FNO | 0.023144 | −322.466508 (−42.3) | −322.673125 (−42.2) | −42.5 |
| **P$_3$** FCN+HNO | 0.023647 | −322.440405 (−26.0) | −322.650721 (−28.2) | −28.1 |
| **P$_4$** $N_2$+HFCO | 0.026097 | −322.638384 (−150.2) | −322.840629 (−147.4) | −145.8 |
| **P$_{10}$** CO+$N_2$+HF | 0.019522 | −322.638980 (−150.6) | −322.831953 (−141.9) | −144.4 |
| **P$_{16}$** F+HCN+NO | 0.024120 | −322.373865 (15.8) | −322.580691 (15.8) | 16.1 |
| **P$_{17}$** H+FCN+NO | 0.017802 | −322.366236 (20.6) | −322.572415 (20.9) | 17.3 |
| **P$_{18}$** F+$N_2$+HCO | 0.018219 | −322.444878 (−28.8) | −322.646014 (−25.2) | −28.6 |
| **P$_{19}$** H+$N_2$+FCO | 0.013436 | −322.475375 (−47.9) | −322.674743 (−43.2) | −49.6 |
| **a$_1$** | 0.029366 | −322.469766 (−44.4) | −322.686946 (−50.9) | −47.3 |
| **a$_2$** | 0.029378 | −322.471947 (−45.8) | −322.689156 (−52.3) | −48.6 |
| **a$_3$** | 0.029317 | −322.468802 (−43.8) | −322.686234 (−50.5) | −46.8 |
| **b** | 0.031529 | −322.468488 (−43.6) | −322.686739 (−50.8) | −45.8 |
| **c$_1$** | 0.030808 | −322.402590 (−2.2) | −322.617773 (−7.5) | −3.0 |
| **e** | 0.032150 | −322.426418 (−17.2) | −322.630912 (−15.8) | −10.4 |
| **i** | 0.031729 | −322.444590 (−28.6) | −322.651377 (−28.6) | −23.5 |
| **j$_1$** | 0.029677 | −322.368103 (19.4) | −322.587515 (11.5) | 15.3 |
| **l$_1$** | 0.028425 | −322.398923 (0.1) | −322.622702 (−10.6) | −7.5 |
| **m$_1$** | 0.029123 | −322.421740 (−14.3) | −322.640820 (−22.0) | −18.5 |
| **TSa$_1$a$_2$** | 0.028624 | −322.445063 (−28.9) | −322.661687 (−35.1) | −31.9 |
| **TSa$_1$m$_1$** | 0.021226 | −322.355648 (27.2) | −322.565327 (25.4) | 23.9 |
| **TSa$_1$P$_1$** | 0.025402 | −322.424287 (−15.9) | −322.638330 (−20.4) | −19.3 |
| **TSa$_1$P$_2$** | 0.025819 | −322.422311 (−14.6) | −322.626778 (−13.2) | −11.7 |
| **TSa$_2$a$_3$** | 0.028734 | −322.460481 (−38.6) | −322.679497 (−46.2) | −43.0 |
| **TSa$_2$c$_1$** | 0.025913 | −322.384312 (9.2) | −322.598641 (4.5) | 6.0 |
| **TSa$_2$i** | 0.029189 | −322.403953 (−3.1) | −322.618958 (−8.3) | −4.7 |
| **TSa$_2$P$_1$** | 0.026211 | −322.426677 (−17.4) | −322.638860 (−20.7) | −19.1 |
| [a]**TSa$_2$P$_3$** | 0.022286 | −323.165262 | −322.606973 (−0.7) | −1.5 |
| **TSa$_3$b** | 0.030040 | −322.425716 (−16.8) | −322.644180 (−24.1) | −20.0 |
| **TSa$_3$l$_1$** | 0.025802 | −322.381653 (10.9) | −322.604635 (0.7) | 2.1 |
| **TSbe** | 0.026896 | −322.373384 (16.1) | −322.581781 (15.1) | 17.2 |
| **TSbP$_4$** | 0.028970 | −322.442378 (−27.2) | −322.663011 (−35.9) | −32.5 |
| **TSij$_1$** | 0.025884 | −322.351461 (29.8) | −322.563078 (26.8) | 28.3 |
| **TSiP$_4$** | 0.028604 | −322.329137 (43.9) | −322.577280 (17.9) | 21.1 |
| **TSRa$_3$** | 0.027201 | −322.386553 (7.8) | −322.587926 (11.2) | 13.5 |
| **TSRi** | 0.027129 | −322.373409 (16.1) | −322.577346 (17.9) | 20.1 |
| **TSRP$_4$-NO** | 0.027359 | −322.364562 (21.6) | −322.576100 (18.6) | 21.0 |
| **TSRP$_4$-O** | 0.026463 | −322.364042 (21.9) | −322.578889 (16.9) | 18.7 |
| **TSP$_1$P$_{16}$** | 0.026983 | −322.364195 (21.9) | −322.578893 (16.9) | 19.0 |
| **TSP$_1$P$_{17}$** | 0.021437 | −322.336310 (39.4) | −322.562553 (27.1) | 25.8 |
| **TSP$_4$P$_{10}$** | 0.020529 | −322.552911 (−96.6) | −322.751571 (−91.5) | −93.4 |

[a] The calculated results at the QCISD(T)/6-311G(2df,p)//B3LYP/6-311G(d,p) level.

of **TSa$_2$P$_3$** (−1.5 kcal/mol). Furthermore, since **TSa$_1$P$_2$** in **Path P$_2$** lies higher than **TSa$_1$P$_1$** in **Path1 P$_1$**, **TSa$_2$P$_1$** in **Path2 P$_1$**, and **TSa$_3$b** in **Path P$_4$**, **Path P$_2$** is the second uncompetitive reaction pathway. It seems very difficult to compare the feasibility of **Path1 P$_1$**, **Path2 P$_1$,** and **Path P$_4$** without the detailed dynamic calculation. The relative energies of the determining rate transition states for three reaction pathways are very similar, i.e., **TSa$_1$P$_1$** (−19.3) in **Path1 P$_1$**, **TSa$_2$P$_1$** (−19.1) in **Path2 P$_1$**, and **TSa$_3$b** (−20.0) in **Path P$_4$**. Then, we tentatively expect that these three pathways may have, a comparable contribution to the $^1$CHF+$N_2$O reaction, i.e., among the final product distributions, the branching ratio of **P$_1$** HFCN+NO may be twice as many as that of **P$_4$** $N_2$+HFCO. However, as shown in Figure 4c, the formation of **P$_4$** requires surmounting the barriers of the other transition states **TSa$_1$a$_2$** (15.4 kcal/mol) and **TSbP$_4$** (13.3 kcal/mol) except **TSa$_3$b** (26.8 kcal/mol). It will kinetically hinder the formation of **P$_4$**. On the other hand, **P$_1$** lies considerably higher in energy than **P$_4$**, even than **P$_2$** and **P$_3$**. Thermodynamically, the formation of **P$_4$** is more favorable than **P$_1$**. Thus, the actual yields of the products may depend on the reaction condition in the experiment.

As a result, reflected in final product distributions, we predict that (1) a total of four kinds of products **P$_1$** HFCN+NO, **P$_2$** HCN+FNO, **P$_3$** FCN+HNO, and **P$_4$** $N_2$+HFCO should be observed; (2) **P$_1$** may be the most feasible product with a largest yield; (3) **P$_4$** may be the second favorable product with the branching ratio which may quantitatively be half of that of **P$_1$**; (4) **P$_2$** may be the third feasible products; (5) **P$_3$** is the least competitive product.

It is useful to make comparison for the mechanism of the title reaction between B3LYP-calculated and MP2-calculated results. Except for **TSa$_2$P$_3$**, the stationary points of the most relevant reaction pathways at the B3LYP/6-31G(d,p) level are also obtained at the MP2/6-311G(d,p) level. At the QCISD(T)/6-311G(d,p)//B3LYP/ 6-31G(d,p) level, we predict that (1) **P$_1$** HFCN+NO may be the most feasible product with a considerable large yield; (2) **P$_2$** HCN+FNO and **P$_4$** $N_2$+HFCO may be the second feasible products which have the comparable branching ratios, (3) **P$_3$** FCN+HNO should be the least favorable product. Generally, the B3LYP-calculated and MP2-calculated results are in agreement. A very small discrepancy lies in the formation pathways of **P$_1$** and **P$_4$**. At the MP2/6-311G(d,p) level, the formation pathway of **P$_4$** may be comparable with each of these of **P$_1$**, while at the B3LYP/6-31G(d,p) level, the formation pathway of **P$_4$** cannot compete with each of these of **P$_1$**.

**3.3. Experimental Implications.** The initial step in five feasible reaction pathways above-mentioned is a barrier-consumed end-N attack process with a considerable barrier of 13.5 kcal/mol at the QCISD(T)/6-311G(2df,p)//MP2/6-311G-(d,p)+ZPE level. By means of our calculated potential energy surface, we roughly estimate the theoretical rate constants of the initial step, i.e., $^1CHF+N_2O$ **R** → HFCNNO **a**$_1$ based on the simple transition state theory. The rate constant formula $K = kT/h\ e^{\Delta S/R}e^{\Delta E/RT}$ is used, where $k$, $\Delta S$, and $\Delta E$ denote the rate constant, entropy difference, and barrier height, respectively. On the basis of the calculated values $\Delta S = -0.033578$ kcal mol$^{-1}$ K$^{-1}$, $\Delta E = 13.5$ kcal/mol, we can obtain the rate constant $6.0 \times 10^{-23}$ cm$^3$ molecule$^{-1}$ s$^{-1}$ at $T = 295$ K. It should be pointed out that once such a high-energy transition state **TSRa**$_1$ is surmounted, the title reaction will enter the potential well with about 47.3 kcal/mol energy and subsequently some important reaction pathways lie below the reactants **R**. As a result, we expect that **TSRa**$_1$ is the rate-determining transition state for the total reaction and the calculated rate constant $6.0 \times 10^{-23}$ cm$^3$ molecule$^{-1}$ s$^{-1}$ can represent roughly the low reactivity of the title reaction. However, the rate constant of the title reaction in the experiment is measured to be $(2.55 \pm 0.15) \times 10^{-12}$ cm$^3$ molecule$^{-1}$ s$^{-1}$ at $T = 295$ K.[11] Clearly, such an experimental measurement cannot be consistent with our calculated result. On the other hand, since the available energy of 13.5 kcal/mol is required to drive the reaction to proceed, the title reaction may be important in high-temperature processes. Thus, it is very desirable to perform experimental measurements on the high-temperature rate constants for the title reaction in the future.

**3.4. Comparison with the $^1CH_2+N_2O$ Reaction.** It is worthwhile to compare the potential energy surface feature of the title reaction with that of the analogous $^1CH_2+N_2O$ reaction. Very recently, Liu et al.[27] performed a detailed theoretical investigation on the $^1CH_2+N_2O$ reaction. The initial step is an end-N attack on the C-atom to form $H_2CN_2O$ (*cis*- or *trans*-) with no barrier. Sequentially, $H_2CN_2O$ (*cis*- or *trans*-) can dissociate to $H_2CN+NO$ via the direct N−N bond rupture or HCN+HNO via the concerted N−N bond cleavage and H-shift. These two primary products can further dissociate to form the final product HCN+NO+H. In addition, *cis*-$H_2CN_2O$ can alternatively take a ring-closure leading to the four-membered ring isomer followed by dissociation to $N_2+H_2CO$. The products HCN+NO+H and $N_2+H_2CO$ can be formed with a comparable branching ratio. A notable finding is that $N_2+H_2CO$ can be formed via a side N−O $\pi$ bonding attack at high temperatures.

Generally, the potential energy surface features of the $_1CHF+N_2O$ reaction are quite in parallel to those of the $^1CH_2+N_2O$ reaction. First, a significant discrepancy lies in the initial association. In the title reaction, the end-N attack on the C-atom to form HFCNNO **a**$_1$ requires overcoming the barrier of 13.5 kcal/mol, whereas in the $^1CH_2+N_2O$ reaction the same association is predicted to be a barrierless process. It may be reasonably interpreted that the reactivity of the $^1CHF+N_2O$ reaction is lower than the $^1CH_2+N_2O$ reaction. Second, in the $^1CH_2+N_2O$ reaction, the concerted H-shift and N−N bond cleavage to form product HCN+HNO plays an important role in the total reaction. However, in the $^1CHF+N_2O$ reaction, we obtain the concerted F-shift and N−N bond dissociation to form HCN+FNO as well as the concerted H-shift and N−N bond rupture leading to FCN+HNO. By comparison, it is found that the former is more feasible the later. However, these two concerted processes cannot compete with the formation pathways of **P**$_1$ HFCN+NO and **P**$_4$ $N_2$+HFCO. Third, For the $^1CH_2+N_2O$ reaction, two important primary products $H_2CN$+NO and HCN+HNO can further dissociate to give HCN+NO+H, whereas for the $^1CHF+N_2O$ reaction, the secondary dissociation reactions of three feasible primary products **P**$_1$ HFCN+NO, **P**$_2$ HCN+FNO, and **P**$_3$ FCN+HNO leading to **P**$_{16}$ F+HCN+NO or **P**$_{17}$ H+FCN+NO are thermodynamically forbidden. Undoubtedly, it decreases the formation of NO and thus may play an important role in NO-reduction process. Finally, in the $^1CH_2+N_2O$ reaction, the transition state of the side NO-$\pi$-bond attack leading to $N_2+H_2CO$ is 5.1 kcal/mol higher than the reactants. As a result, such a process can take place at high temperatures. However, in the $^1CHF+N_2O$ reaction, the similar transition state **TSRP**$_4$**-NO** lies 21.0 kcal/mol above the reactants. Even at high temperatures, it is impossible for such a process to take place.

## 4. Conclusions

A detailed singlet potential energy surface of the $^1CHF+N_2O$ reaction system is carried out at the B3LYP and QCISD(T) (single-point) levels. Further, the stationary points of the relevant reaction pathways are calculated at the QCISD(T)/6-311G-(2df,p)//MP2/6-311G(d,p) level. The main calculated results can be summarized as follows:

(1) The most feasible initial association way is the end-N attack of $^1CHF$ at $N_2O$ leading to HFCNNO **a**$_1$ via the transition state **TSRa**$_1$ with the barrier of 13.5 kcal/mol. Yet, the other attacks including end-O, side N−N $\pi$ bonding, and side N−O $\pi$ bonding are considerable barrier-consumed ways, indicative of their negligible contribution at normal temperature.

(2) Starting from HFCNNO **a**, four kinds of products can be obtained, i.e., **P**$_1$ HFCN+NO, **P**$_2$ HCN+FNO, **P**$_3$ FCN+HNO, and **P**$_4$ $N_2$+HFCO. Among these products, **P**$_1$ is the most favorable product with a large branching ratio which may be twice as many as the second feasible product **P**$_4$. **P**$_2$ is less feasible than **P**$_1$ and **P**$_4$. **P**$_3$ is the least feasible product. These four products cannot further dissociate due to thermodynamical and kinetic factors. By comparison, it is found that the B3LYP-calculated and MP2-calculated results are generally in agreement.

(3) Our calculated potential energy surface of $^1CHF+N_2O$ reaction is compared with that of the analogous $^1CH_2+N_2O$ reaction. Both the potential energy surface features are very alike. The discrepancies between two reactions are discussed.

**Acknowledgment.** This work is supported by the National Natural Science Foundation of China (No. 29892168, 20073014, 20103003).

## References and Notes

(1) *Halon Replacements*; Miziolek, A. W., Tsang, W., Eds.; ACS Symp. Ser. 611; American Chemical Society: Washington, DC, 1995.
(2) Brownsword, R. A.; Hancock, G.; Heard, D. E. *J. Chem. Soc. Faraday Trans.* **1991**, *87*, 2283.
(3) Cookson, J. L.; Hancock, G.; Mckendrick, K. G. *Ber. Bunsen-Ges., Phys. Chem.* **1985**, *89*, 335.
(4) Hancock, G.; Ketley. G. W.; MacRobert, A. J. *J. Phys. Chem.* **1984**, *88*, 2104.
(5) Herron, J. T. *J. Phys. Chem. Ref. Data* **1988**, *17*, 967.
(6) Tsai, C.; McFadden, D. L. *J. Phys. Chem.* **1990**, *94*, 3298.
(7) Zárate, A. O.; Martinez, R.; Rayo, M. N. S.; Castano, F.; Hancock, G. *J. Chem. Soc., Faraday Trans.* **1992**, *88*, 535.
(8) Hancock, G.; Ketley, G. W. *J. Chem. Soc., Faraday Trans.* **1982**, *78*, 1283.
(9) Browsword, R. A.; Hancock, G.; Oum, K. W. *J. Phys. Chem.* **1996**, *100*, 4840.
(10) Haynes, B. S. *Combust. Flame* **1977**, *113* (28), 81.
(11) Fernandez, J. A.; Martinez, R.; Sanchez Rayo, M. N.; Castano, F. *An. Quim. Int. Ed.* **1997**, *93*, 22.
(12) Koch, M.; Temps, F.; Wagener, R.; Wagner, H. Gg. *Ber. Bunsen-Ges. Phys. Chem.* **1990**, *94*, 645.

(13) Hancock, G.; Ketley, G. W. *J. Chem. Soc., Faraday Trans*. **1982**, *78*, 1283.
(14) Browsword, R. A.; Hancock, G.; Oum, K. W. *J. Phys. Chem*. **1996**, *100*, 4840.
(15) Liu, J. J.; Ding, Y. H.; Feng, J. K.; Sun, C. C. *J. Phys. Chem. A* **2001**, *105*, 9901.
(16) Grussdorf, F.; Temps, F.; Wagner, H. G. *Ber. Bunsen-Ges. Phys. Chem*. **1997**, *101*, 134.
(17) Roggenbuck, J.; Temps, F. *Chem. Phys. Lett*. **1998**, *285*, 422.
(18) Laufer, A. H.; Bass, A. M. *J. Phys. Chem*. **1974**, *78*, 1344.
(19) Vinckier, C.; Debruyn, W. *J. Phys. Chem*. **1979**, *83*, 2057.
(20) Seidler, V.; Temps, F.; Wagner, H. Gg.; Wolf, M. *J. Phys. Chem*. **1989**, *93*, 1070.
(21) Atakan, B.; Kocis, D.; Wolfrum, J.; Nelson, P. In *24th Symposium (International) on Combustion*; The Combustion Institute: Pittsburgh, PA, 1992; p 691.
(22) Bauerle, S.; Klatt, M.; Wagner, H. Gg. *Ber. Bunsen-Ges. Phys. Chem*. **1995**, *99*, 97.
(23) Shapley, W. A.; Bacskay, G. B. *Theor. Chem. Acc*. **1998**, *100*, 212.
(24) Shapley, W. A.; Bacskay, G. B. *J. Phys. Chem. A* **1999**, *103*, 4505.
(25) Shapley, W. A.; Bacskay, G. B. *J. Phys. Chem. A* **1999**, *103*, 4514.
(26) Frisch, M. J.; Trucks, G. W.; Schlegel, H. B.; Scuseria, G. E.; Robb, M. A.; Cheeseman, J. R.; Zakrzewski, V. G.; Montgomery, J. A.; Stratmann, R. E., Jr.; Burant, J. C.; Dapprich, S.; Millam, J. M.; Daniels, A. D.; Kudin, K. N.; Strain, M. C.; Farkas, O.; Tomasi, J.; Barone, V.; Cossi, M.; Cammi, R.; Mennucci, B.; Pomelli, C.; Adamo, C.; Clifford, S.; Ochterski, J.; Petersson, G. A.; Ayala, P. Y.; Cui, Q.; Morokuma, K.; Malick, D. K.; Rabuck, A. D.; Raghavachari, K.; Foresman, J. B.; Cioslowski, J.; Ortiz, J. V.; Stefanov, B. B.; Liu, G.; Liashenko, A.; Piskorz, P.; Komaromi, I.; Gomperts, R.; Martin, R. L.; Fox, D. J.; Keith, T.; Al-Laham, M. A.; Peng, C. Y.; Nanayakkara, A.; Gonzalez, C.; Challacombe, M.; Gill, P. M. W.; Johnson, B.; Chen, M.; Wong, W.; Andres, J. L.; Gonzalez, C.; Head-Gordon, M.; Replogle, E. S.; Pople, J. A. *G98W A.7*; Gaussian, Inc.: Pittsburgh, PA, **1998**.
(27) Liu, J. J.; Feng, J. K.; Ding, Y. H.; Ren, A. M.; Wang, S. F.; Sun, C. C. *J. Phys. Chem. A* **2001**, *105*, 5885.